Focused on the research activities of the Greek Society of Experimental Mechanics of Materials

Visual Abstract

Imaging performance of a $CaWO_4$/CMOS sensor

Niki Martini, Vaia Koukou, George Fountos, Ioannis Valais, Ioannis Kandarakis, Christos Michail
Radiation Physics, Materials Technology and Biomedical Imaging Laboratory, Department of Biomedical Engineering, University of West Attica, Athens 12210, Greece
michail@upatras.gr, http://orcid.org/0000-0001-5863-8013

Athanasios Bakas, Eleftherios Lavdas, Konstantinos Ninos, Georgia Oikonomou, Lida Gogou
Department of Biomedical Sciences, University of West Attica, Athens 12210, Greece

George Panayiotakis
Department of Medical Physics, Faculty of Medicine, University of Patras, 265 00 Patras, Greece

ABSTRACT. The aim of this study was to investigate the modulation transfer function (MTF) and the effective gain transfer function (eGTF) of a non-destructive testing (NDT)/industrial inspection complementary metal oxide semiconductor (CMOS) sensor in conjunction with a thin calcium tungstate ($CaWO_4$) screen. Thin screen samples, with dimensions of 2.7x3.6 cm^2 and thickness of 118.9 μm, estimated from scanning electron microscopy-SEM images, were extracted from an Agfa Curix universal screen and coupled to the active area of an active pixel (APS) CMOS sensor. MTF was assessed using the slanted-edge method, following the IEC 62220-1-1:2015 method. MTF values were found high across the examined spatial frequency range. eGTF was found maximum when $CaWO_4$ was combined with charge-coupled devices (CCD) of broadband anti-reflection (AR) coating (17.52 at 0 cycles/mm). The combination of the thin $CaWO_4$ screen with the CMOS sensor provided very promising image resolution and adequate efficiency properties, thus could be also considered for use in CMOS based X-ray imaging devices, for various applications.

KEYWORDS. $CaWO_4$; Phosphors; Medical imaging; APS; CMOS sensors; MTF.

OPEN ACCESS

Citation: Martini, N., Koukou, V., Fountos, G., Valais, I., Kandarakis, I., Michail, Ch., Bakas, A., Lavdas, E., Ninos, K., Oikonomou, G., Gogou, L., Panayiotakis, G., Imaging performance of a $CaWO_4$/CMOS sensor, Frattura ed Integrità Strutturale, 50 (2019) 471-480.

Received: 22.01.2019
Accepted: 22.05.2019
Published: 01.10.2019

INTRODUCTION

Phosphor materials made of calcium tungstate ($CaWO_4$) [1,2] and zinc sulfide (ZnS) were used as radiation detectors, in the form of thin screens, for almost a century [3,4]. $CaWO_4$ is a low cost, very stable material, but with a decay time not ideal for applications that require high counting rate measurements (Table 1) [5]. $CaWO_4$ emits light in

the blue region of the spectrum which provides excellent compatibility with photocathodes, incorporated in various types of photomultipliers (PMTs), charge-coupled devices (CCD), as well as, with non-passivated amorphous hydrogenated silicon photodiode (a-Si:H), employed in thin film transistors of active matrix flat panel detectors [5]. When rare earth phosphors came into the spot-light, $CaWO_4$ was dis-continued for medical imaging applications. Thereafter, terbium-doped gadolinium oxysulfide (Gd_2O_2S:Tb) rare earth phosphor, and later cesium iodide (CsI) were established for digital imaging applications (medical, industrial radiography, etc.) including CCDs and complementary metal oxide semiconductors (CMOS) [3,4,6-11]. In industrial radiography, non-destructive testing (NDT) is used; it consists of a variety of non-invasive inspection techniques that is used to evaluate material properties, components, or entire process units. Radiographic testing is one of the most frequently used NDT techniques that involve the use of X-rays and digital detector systems, such as amorphous silicon, CCDs and CMOS sensors [12-14]. However, beyond the dominance of terbium-doped gadolinium oxysulfide, the interest for $CaWO_4$ has been renewed in applications such as, particle astrophysics in the quest for dark matter in the universe [15-17], for WIMP-nucleon elastic scattering interactions [18,19], as well as, for customs and border control [15,20]. The resolution properties of this material [21,22], along with the adequate luminescence emission efficiency, at specific X-ray energies [5] could be also considered for dual energy applications [23-28].

All the aforementioned applications require efficient detectors, of high resolution, with good spectral matching between the phosphor's emission light and the sensitivity of the sensor, thus the aim of this study is to investigate further the properties of a thin layered calcium tungstate screen, coupled to a state-of-the-art NDT active pixel sensor (APS) CMOS sensor, in order to enhance the imaging capabilities of the integrated detector.

Measurements were conducted, following standardized methodologies for medical imaging configurations (sensors and scintillator material combinations) [11]. Standardized protocols were used for both resolution and efficiency measurements [5, 29-31]. The latest IEC 62220-1-1:2015 protocol from the International Electrotechnical Commission (IEC) 62220 series was used [32,33].

MATERIALS AND METHODS

Phosphor screens

Samples of $CaWO_4$ were extracted from an Agfa Curix universal screen. For the resolution measurements samples with dimensions 2.7x3.6 cm^2 were used. The phosphor is used in the intensifying screens employed in X-ray imaging [31,34,35]. The internal properties of the samples were examined via scanning electron microscopy (SEM) [36].

X-ray absorption (@50keV)	35%
Light conversion efficiency	4-5%
Melting point	1570-1670 ^oC
Molar mass	287.9156 g/mol
Atomic number	74
Density	6.06-6.1 g/cm^3
Afterglow	From $5x10^{-6}$ sec up to a few sec
Refractive index	1.94
K-edge	69.5 keV
Decay time	$6-8x10^3$ ns

Table 1: $CaWO_4$ properties [3-5,15,17,37,38].

Scanning electron microscopy (SEM)

Parameters such as particle size and thickness of the $CaWO_4$ compound were verified via SEM micrographs using the Jeol JSM 5310 scanning electron microscope and the INCA software. Within this system, gold can be used to image a site of interest of the sample. For the elementary particle analysis, a carbon thread evaporation process was used. Carbon was flash evaporated under vacuum conditions to produce a film suited for the $CaWO_4$ SEM specimen in a BAL-TEC CED 030 carbon evaporator (~10^{-2} mbar) [36].

CMOS sensor

The $CaWO_4$ scintillating screen was manually coupled to an optical readout device including a CMOS Remote RadEye HR photodiode pixel array [39]. The CMOS photodiode array consists of 1200x1600 pixels with 22.5 μm pixel spacing. This sensor was initially manufactured for non-destructive testing (NDT)/industrial inspection applications especially for tight or difficult to reach spaces. However, due it its unique resolution properties can be also used in medical imaging applications. Thus, it would be of interest to integrate a scintillating material that came to the spotlight once again, with this state-of-the-art sensor in order to further exploit their imaging characteristics. The $CaWO_4$ screen was directly overlaid onto the active area of the CMOS and irradiated with a BMI General Medical Merate tube having rotating Tungsten anode and inherent filtration equivalent to 2 mm Al at 70 kV (RQA-5) X-ray beam quality and source to detector distance of 156 cm [21].

Modulation Transfer Function (MTF)

The modulation transfer function (MTF) was measured by irradiating a PTW Freiburg tungsten edge test device, following the procedures described in the IEC standard [11,32,33]. The updated IEC 62220-1-1:2015 [11,33,40] standard describes certain modifications, such as the method for the determination of the modulation transfer function (MTF) in which the final MTF can be now obtained only through averaging of the oversampled edge spread function (ESF) [33,41-43]. The average of all oversampled ESFs was then fitted with a modified Fermi-Dirac distribution function as follows [11,21]:

$$Fermi(x) = \left(\frac{c}{e^{(x-a)/b} + 1} \right) + d \tag{1}$$

The values of fitting parameters are a=7200, b=15, c=65500 and d=0. The fitted ESF was differentiated to obtain the line spread function (LSF) and Fourier transformed to finally obtain the MTF [21,44].

Luminescence efficiency measurements

The efficiency (output signal) of a scintillator to emit light, upon X-ray irradiation is experimentally determined by measuring the emitted light energy flux $\dot{\Psi}_\lambda$ and the exposure rate ($\dot{X}$) using a calibrated dosimeter. In this study, the Piranha P100B RTI was used. The light flux measurements were performed using a light integration sphere (Oriel 70451), coupled to a photomultiplier (PMT) (EMI 9798B) and connected to a Cary 401 vibrating reed electrometer [5,9]. The circular $CaWO_4$ sample was also exposed to X-rays on the BMI General Medical Merate tube, with energies ranging from 50 to 125 kVp. An additional 20 mm Al filtration was introduced in the beam to simulate beam quality alternation by a human body [45,46].

X-ray luminescence efficiency (XLE)

The X-ray luminescence efficiency (XLE) is a unitless measure of the fraction of incident energy converted into emitted light energy, i.e. the ratio of the emitted light energy flux over the incident X-ray energy flux ($\eta_\psi = \Psi_A/\Psi_0$). XLE was determined [9] by converting the measured X-ray exposure data into X-ray energy flux (Ψ_0) [9], as follows: $\Psi_0 = X\hat{\Psi}$ where $\hat{\Psi}$ is defined as the X-ray energy flux per exposure rate, estimated according to Eq.(2) [5,36]:

$$\hat{\Psi} = \frac{\int \Psi_0(E)dE}{\int \Psi_0(E)\left[X/\Psi_0(E)\right]dE} \tag{2}$$

where

$$X/\Psi_0(E) = (\mu_{en}(E)/\rho)_{air} \cdot (W_A/e)^{-1} \tag{3}$$

is the factor converting energy flux into exposure rate, $(\mu_{en}/\varrho)_{air}$ the X-ray mass energy absorption coefficient of air, at energy E, and (W_A/e) is the average energy per unit of charge required to produce an electron-ion pair in air. (W_A/e) and $(\mu_{en}/\varrho)_{air}$ were obtained from tabulated data [47].

Detector quantum optical gain (DQG)

Detector quantum optical gain (DQG) is the ratio of the light photon flux (Φ_A) over the X-ray photon flux (Φ_X) and expresses the emission efficiency in terms of quantum gain (number of emitted light photons per incident X-ray). Using this quantity, the emitted light photon fluence can be expressed in terms of experimentally determined quantities (absolute efficiency, exposure, mean light wavelength), by using Eq.(4) [5]:

$$\Phi_{\Lambda} = \Psi_{\Lambda} \Big/ hc\bar{\lambda}^{-1} \tag{4}$$

Φ_X was determined by using Eqs.(2,3), replacing Ψ_0 by Φ_0 and dividing Eq.(3) by the X-ray energy [9]. Eqs(2,4) may be expressed in the spatial frequency domain. Within this framework the detector quantum gain may be expressed by a gain transfer function (GTF), defined as follows [36,45]:

$$GTF(E_0, v, w) = \Phi_{\Lambda}(E_0, v, w) / \Phi_0 \tag{5}$$

where v denotes spatial frequency, w coating thickness and $\Phi_A(E_0,v,w)$ is the spatial frequency-dependent emitted light photon fluence. Gain transfer function, can be expressed through the MTF [36,45]:

$$GTF(v, w) = MTF(v, w) \cdot DQG \tag{6}$$

where DQG is the detector quantum optical gain. In medical imaging, where fluorescent screens are used in combination with optical detectors (films in the past, photocathodes, photodiodes), the spectral matching between the emitted phosphor light and the optical detector sensitivity must be considered. This is because the degree of spectral matching affects the amount of light utilized to form the final image. Thus, Eq.(6) is reduced by a factor a_S, expressing the fraction of emitted light that can be detected by the optical detector, which exhibits a specific spectral distribution of sensitivity. a_S, can be calculated by Eq.(7) [5,45]:

$$a_S = \frac{\int S_P(\lambda) S_D(\lambda) d\lambda}{\int S_P(\lambda) d\lambda} \tag{7}$$

where $S_P(\lambda)$ is the spectrum of the light emitted by the phosphor and $S_D(\lambda)$ is the spectral sensitivity of the optical detector coupled to the phosphor [5]. By considering a_S, we may define the effective gain transfer function as follows [36,45]:

$$eGTF(v, w) = DQG \cdot MTF(v, w) \cdot a_S \tag{8}$$

RESULTS AND DISCUSSION

Fig.1 shows the grain-size deposition per thickness of $CaWO_4$, estimated from scanning electron microscope images. Qualitatively the mean particle size of $CaWO_4$ phosphor (6.02 μm) was estimated from the SEM images using the ImageJ analysis software, as shown from the grain-size distribution [48,49]. The calculated screen thickness was equal to 118.9 μm estimated by profile measurements on the area depicted as inset in Fig.1, across the material coating [5,22]. Furthermore, in Fig.1 the energy dispersive X-ray (EDX) analysis of the material is demonstrated. It was found that $CaWO_4$ was dominantly present in the sample along with carbon (C) due to the carbon thread evaporation process. Normalized stoichiometric results, obtained by the SEM on the region of interest (ROI) of Fig.1, showed the following % weights of the elements in the mixture: Calcium (Ca) 5.77%, oxygen (O) 26.54%, tungsten (W) 29.94 and carbon due to the carbon thread evaporation process 37.75% [22].

The X-ray characteristic curves (output signal versus incident exposure) of $CaWO_4$ and (for comparison purposes) of a flexible fluorescent Gd_2O_2S:Tb sample (gold standard for imaging applications) of similar coating thickness (30.8 mg/cm^2 for Gd_2O_2S:Tb versus 36.26 mg/cm^2 for $CaWO_4$) are plotted in Fig.2. These coating thicknesses were calculated assuming densities of 7.3 g/cm^3 for Gd_2O_2S:Tb and 6.1 g/cm^3 for $CaWO_4$ with packing densities of 50% for both materials. Results for $CaWO_4$ and Gd_2O_2S:Tb show linear dependence between the output signal and exposure rate in the 4-299 mR/s range. The linear no-threshold fit gave correlation coefficient values R^2 of 0.9997 for $CaWO_4$ and 0.9953 for Gd_2O_2S:Tb, which are very close to unity and indicate that the screens have linear response in this energy range. Gd_2O_2S:Tb was found with clearly higher output signal values than those of $CaWO_4$ due to its higher absolute efficiency values [5].

Fig.3 shows all the oversampled ESFs (Fig.3a) used to create the average ESF and then the Fermi-fitted ESF (Fig.3b), as well as, the resulted LSF (Fig.3c), following the IEC 2015 protocol and the edge phantom. The edge test device consists of a 1 mm thick W edge plate (100×75 mm^2) fixed on a 3 mm thick lead plate. Images of the edge, placed at a slight angle in order to avoid aliasing effects, were obtained. Irradiation was performed at 70kVp and 50 mAs for the tube current and

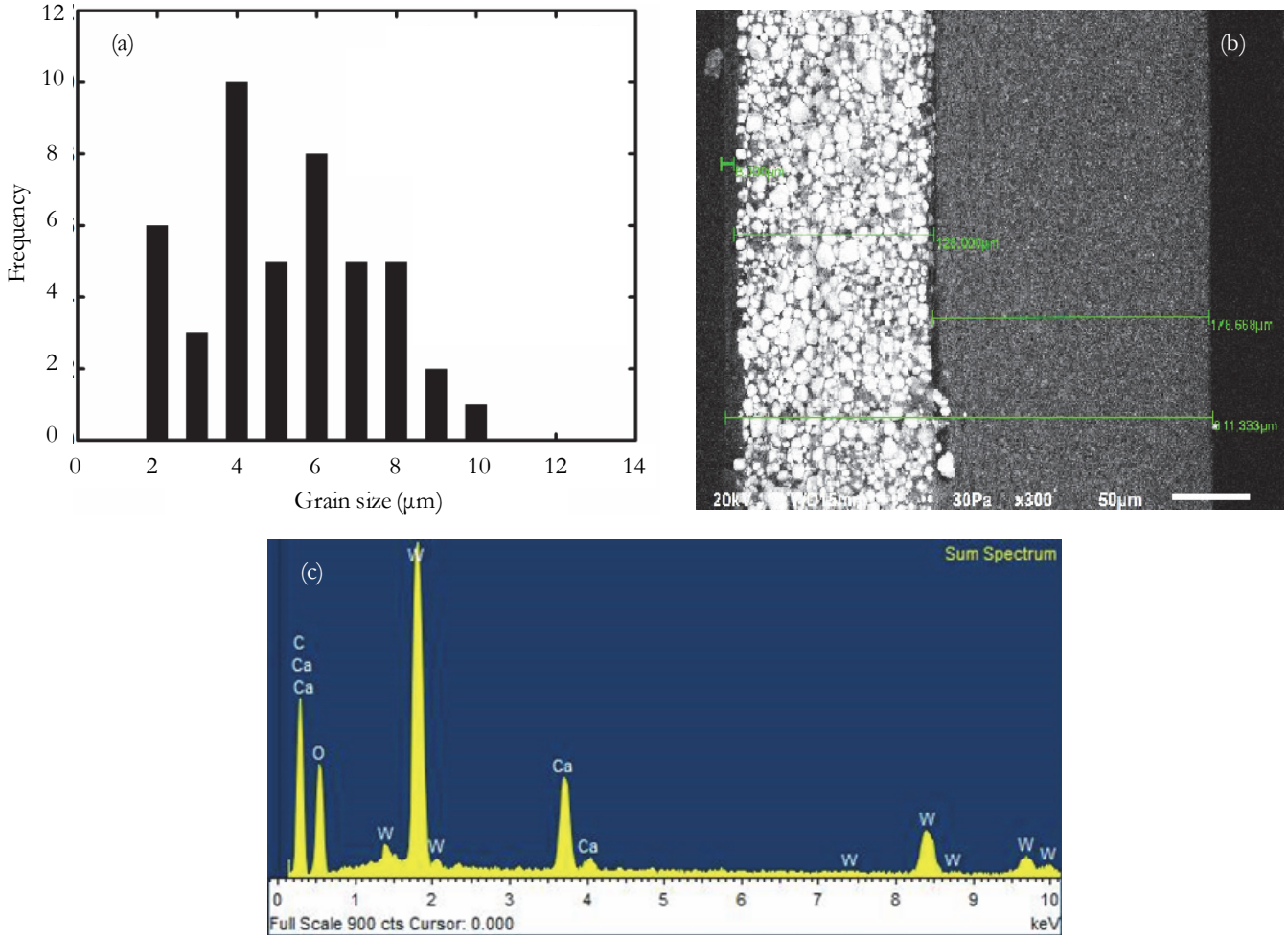

Figure 1: Grain-size distribution obtained from the scanning electron microscope image of the $CaWO_4$ scintillating material (a), obtained from a region of interest (b), along with the energy dispersive X-ray (EDX) analysis (c).

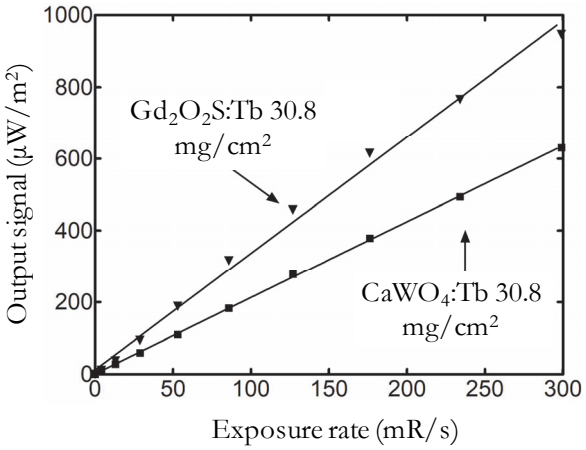

Figure 2: Output signal of the 36.26 mg/cm² $CaWO_4$ screen and a 30.8 mg/cm² Gd_2O_2S:Tb flexible phosphor in the radiographic range of exposures.

exposure time product. This energy is also within the energy range of 51-84 keV that can be utilized for testing steel thicknesses between 2.5 and 12.5 mm [13]. The edge spread function, of the small CMOS detector, was calculated by the extraction of a 2×2 cm² ROI, which covers approximately 41% of the active area of the small area CMOS sensor (2.7×3.6 cm²), with the edge roughly at the center. In the IEC protocol a 5×10cm² ROI is suggested [33]. A smaller ROI may not be

adequate to observe a possible low-frequency sharpness drop in scintillating screens [39]. The variation in the ESF curves that can be depicted from Figs.5(a,b), can be attributed to a statistical noise component mostly prominent at the edge surface area. Fig.3d shows results for the modulation transfer function of the CMOS sensor combined with the 118.9 μm $CaWO_4$ screen, under the RQA-5 (70kVp) beam quality. MTF values were found high across the examined spatial frequency range.

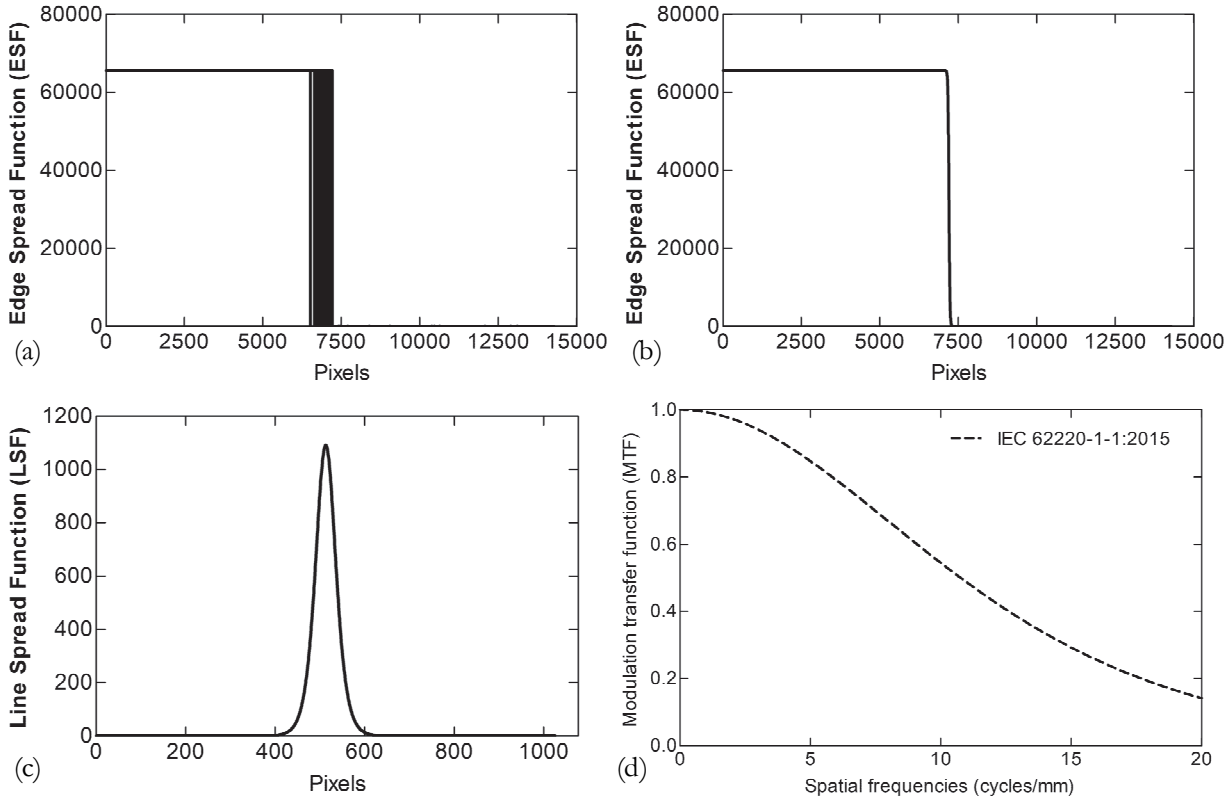

Figure 3: (a) ESFs of a 118.9 μm $CaWO_4$/RadEyeHR CMOS combination, following the IEC 2015 method, (b) averaged and Fermi fitted ESF, (c) LSF, (d) Modulation transfer function following the IEC 2015 protocol, under the RQA-5 beam quality.

Figs.(4,5) show the variation of GTF and eGTF with spatial frequency for the $CaWO_4$ phosphor screen measured at 70 kVp. The difference between this curve and the corresponding MTF curve is due to the influence of X-ray absorption and optical emission on GTF, which are more apparent at lower frequencies. As frequency increases, the influence of MTF on GTF is more significant than the corresponding influence of detector quantum gain (DQG: 18.17 at 70 kVp [5]) causing a further decrease in the GTF (Fig.4).

Figs.5(a-d) shows indicative effective GTF results of the $CaWO_4$ screen with various optical detectors. Results are shown up to 5 cycles/mm, since the measured MTF incorporates the MTF of the CMOS semiconductor which however has been reported to be higher than 0.984, thus the calculation error is minimum [8,50-52]. The best optical detector-screen combination was obtained for a charge-coupled device having broadband anti-reflection (AR) coating (Fig.5c) with an eGTF value of 17.52 at zero spatial frequency. This value reduces GTF only by 3.54% (spectral matching factor: 0.964 [5]). The eGTF values of the CCD, is followed by the Hamamatsu MPPC silicon photomultipliers S10985 (Fig.5b) (eGTF: 17.39 at 0 cycles/mm, matching factor: 0.957), the GaAs photocathode (eGTF: 17.36 at 0 cycles/mm, matching factor: 0.955) (Fig. 5a) and the non-passivated amorphous hydrogenated silicon photodiode (a-Si:H) (Fig.5d) (eGTF: 17.39 at 0 cycles/mm, matching factor: 0.948), employed in thin film transistors in active matrix flat panel detectors.

$CaWO_4$ also shows very good eGTF values with Sensl's silicon PMTs, with eGTF value 14.21 at 0 cycles/mm, for the MicroFM-10035 (matching factor: 0.782), with the MicroFB-30035-SMT (eGTF: 15.25 at 0 cycles/mm, matching factor: 0.839 and with the MicroFC-30035 (eGTF: 15.94 at 0 cycles/mm, matching factor: 0.877 (Fig.5b). Furthermore, it showed very good eGTF with Hamamatsu flat panel position sensitive photomultipliers, such as the H8500C-03 (eGTF: 14.60 at 0 cycles/mm, matching factor: 0.80) (Fig.5c). It is of importance to note that eGTF showed good values when $CaWO_4$ is combined with complementary metal-oxide semiconductors, used in digital radiography and mammography systems, showing maximum when coupled with a hybrid blue CMOS (eGTF: 17.39 at 0 cycles/mm, matching factor: 0.854) [53].

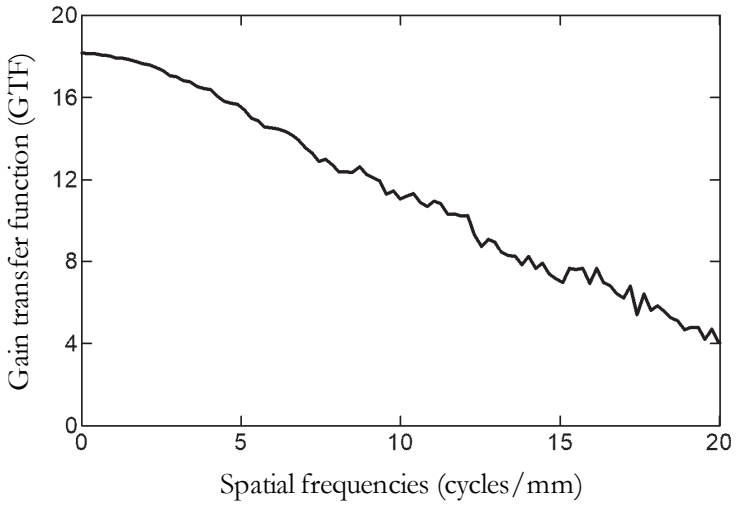

Figure 4: Variation of the GTF with spatial frequency for the thin $CaWO_4$ phosphor screen.

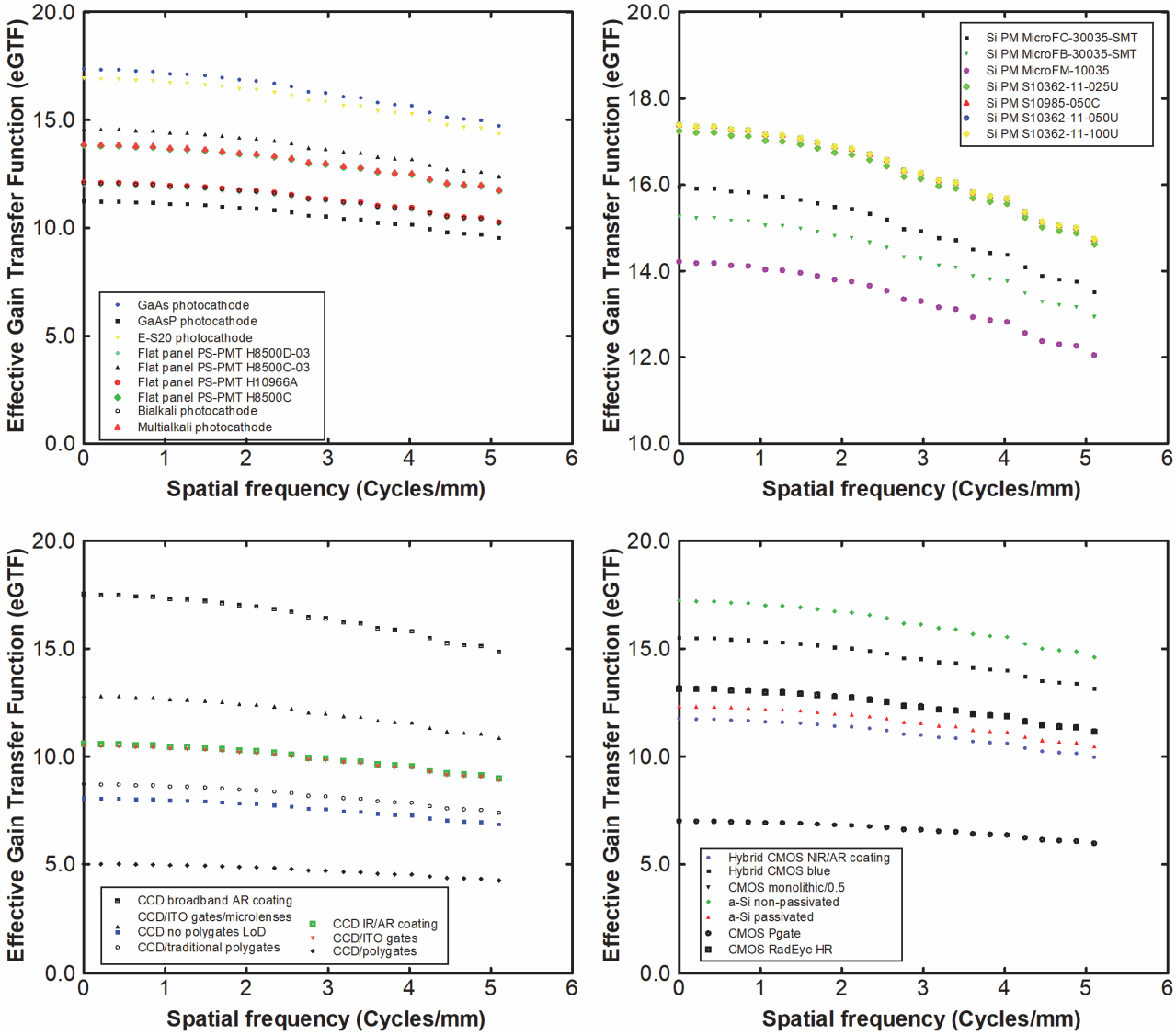

Figure 5: Variation of the eGTF with spatial frequency for the $CaWO_4$ phosphor screen combined with the various optical detectors.

CONCLUSIONS

Applications such as, non-destructive testing, medical imaging etc., require efficient detectors, of high resolution. In this study the resolution properties of a non-destructive testing/industrial inspection CMOS sensor, in conjunction with a scintillating material that came to the spotlight once again ($CaWO_4$) was examined in order to further exploit and enhance the imaging capabilities of an integrated detector, incorporating these two modules. Experiments were carried under X-ray radiography imaging conditions, following the IEC 62220-1-1:2015 protocol.
Furthermore, the detector quantum gain of the screen and the spectral compatibility was also examined for various optical sensor combinations. MTF values of the $CaWO_4$ screen/CMOS combination were found high across the spatial frequency range. As a conclusion, the resolution properties of the thin 118.9 μm $CaWO_4$ screen/CMOS combination are promising for general radiography medical imaging applications.

REFERENCES

[1] Kaugars, G. and Fatouros, P. (1982). Clinical comparison of conventional and rare earth screen-film systems for cephalometric radiographs, Oral, Surg. Oral. Med. Oral. Pathol., 53(3), pp. 322-325.
[2] Derenzo, S., Weber, M., Bourret-Courchesne, E., Klintenberg, M. (2003). The quest for the ideal inorganic scintillator, Nucl. Instr. and Meth. Phys. Res. A., 505, pp. 111-117.
[3] Brixner, L. (1987). New X-Ray Phosphors, Mater, Chem. Phys., 16, pp. 253-281.
[4] Nikl, M. (2006). Scintillation detectors for x-rays, Meas. Sci. Technol., 17, pp. R37-R54.
[5] Michail, C., Valais, I., Fountos, G., Bakas, A., Fountzoula, C., Kalyvas, N., Karabotsos, A., Sianoudis, I., and Kandarakis, I. (2018). Luminescence efficiency of Calcium Tungstate ($CaWO_4$) under X-ray radiation: Comparison with Gd_2O_2S:Tb, Measur., 120, pp. 213-220.
[6] Cavouras, D., Kandarakis, I., Bakas, A., Triantis, D., Nomicos, C., Panayiotakis, G. (1998). An experimental method to determine the effective luminescence efficiency of scintillator-photodetector combinations used in X-ray medical imaging systems, Br. J. Radiol, 71, pp. 766-772.
[7] Cavouras, D., Kandarakis, I., Panayiotakis, G., Kanellopoulos, E., Triantis, D., Nomicos, C. (1998). An investigation of the imaging characteristics of the $Y_2O_2S:Eu^{3+}$ phosphor for application in X-ray detectors of Digital Mammography, Appl. Radiat. Isot, 49, pp. 931-937.
[8] Michail, C.M., Spyropoulou, V. A., Fountos, G. P., Kalyvas, N.I., Valais, I. G., Kandarakis, I.S., Panayiotakis, G.S. (2011). Experimental and Theoretical Evaluation of a High Resolution CMOS Based Detector under X-Ray Imaging Conditions, IEEE Trans. Nucl. Sci, 58(1), pp. 314-322.
[9] Michail, C., Valais, I., Seferis, I., Kalyvas, N., David, S., Fountos, G., Kandarakis, I. (2014). Measurement of the Luminescence properties of Gd_2O_2S:Pr,Ce,F Powder Scintillators under X-ray radiation, Radiat. Meas., 70, pp. 59-64.
[10] Michail, C., Valais, I., Seferis, I., Kalyvas, N., Fountos, G., Kandarakis, I. (2015). Experimental Measurement of a High Resolution CMOS Detector Coupled to CsI Scintillators under X-ray Radiation, Radiat. Meas., 74, pp. 39-46.
[11] Michail, C., Valais, I., Martini, N., Koukou, V., Kalyvas, N., Bakas, A., Kandarakis, I., Fountos, G. (2016). Determination of the Detective Quantum Efficiency (DQE) of CMOS/CsI Imaging Detectors following the novel IEC 62220-1-1:2015 International Standard, Radiat. Meas., 94, pp. 8-17.
[12] Souza, E., Correa, S., Silva, A., Lopes, R., Oliveira, D. (2008). Methodology for digital radiography simulation using the Monte Carlo code MCNPX for industrial applications, Appl. Radiat. Isot., 66, pp. 587-592.
[13] IAEA (2011). Radiation Safety Standard in Industrial Radiography, Specific Safety Guide No. SSg-11. Available at: https://www-pub.iaea.org/books/iaeabooks/8500/Radiation-Safety-in-Industrial-Radiography
[14] Kim, K., Kang, S., Kim, W., Cho, H., Park, C., Lee, D., Kim, G., Park, S., Lim, H., Lee, H., Park, J., Jeon, D., Lim, Y., Je, U., Woo, T. (2018). Improvement of radiographic visibility using an image restoration method based on a simple radiographic scattering model for x-ray nondestructive testing, NDT and E Int., 98, pp. 117-122.
[15] Moszyski, M., Balcerzyk, M., Kraus, H., Czarnacki, W., Mikhailik, V., Nassalski, A., Solskii, I. (2005). Characterization of $CaWO_4$ scintillator at room and liquid nitrogen temperatures, Nucl. Instr. and Meth. Phys. Res. A., 553, pp. 578-591.
[16] Munster, A., Schonert, S., Willers, M. (2017). Cryogenic detectors for dark matter search and neutrinoless double beta decay, Nucl. Instr. and Meth. Phys. Res. A., 845, pp. 387-393.
[17] Zdesenko, Y., Avignone III, F., Brudanin, V., Danevich, F., Nagorny, S., Solsky, I., Tretyak, V. (2005). Scintillation properties and radioactive contamination of $CaWO_4$ crystal scintillators, Nucl. Instr. and Meth. Phys. Res. A., 538, pp. 657-667.

[18] Mikhailik, V., Kraus, H. (2010). Performance of scintillation materials at cryogenic temperatures, Phys. Status. Solidi. B., 247, pp. 1583-1599.
[19] Mikhailik, V., Elyashevskyi, Y., Kraus, H., Kim, H., Kapustianyk, V., Panasyuk, M. (2015). Temperature dependence of scintillation properties of $SrMoO_4$, Nucl. Instr. and Meth. Phys. Res. A., 792, pp. 1-5.
[20] Shahabinejad, H., Feghhi, S., Khorsandi, M. (2014). Structural inspection and troubleshooting analysis of a lab-scale distillation column using gamma scanning technique in comparison with Monte Carlo simulations, Measur., 55, pp. 375-381.
[21] Koukou, V., Martini, N., Valais, I., Bakas, A., Kalyvas, N., Lavdas, E., Fountos, G., Kandarakis, I., Michail, C. (2017). Resolution properties of a Calcium Tungstate ($CaWO_4$) screen coupled to a CMOS imaging detector, J. Phys.: Conf. Ser., 931, pp. 012027.
[22] Martini, N., Koukou, V., Fountos, G., Valais, I., Bakas, A., Ninos, K., Kandarakis, I., Panayiotakis, G., Michail, C. (2018). Towards the enhancement of medical imaging with non-destructive testing (NDT) CMOS sensors. Evaluation following IEC 62220-1-1:2015 international standard, Procedia Structural Integrity, 10, pp. 326-332.
[23] Sotiropoulou, P., Fountos, G., Martini, N., Koukou, V., Michail, C., Kandarakis, I., Nikiforidis, G. (2015). Bone calcium/phosphorus ratio determination using Dual Energy X-ray method, Phys. Med., 31, pp. 307-313.
[24] Koukou, V., Martini, N., Michail, C., Sotiropoulou, P., Fountzoula, C., Kalyvas, N., Kandarakis, I., Nikiforidis, G., Fountos, G. (2015). Dual energy method for breast imaging: A simulation study, Comput. Math. Methods Med., 2015, pp. 574238.
[25] Sotiropoulou, P., Fountos, G., Martini, N., Koukou, V., Michail, C., Kandarakis, I., Nikiforidis, G. (2016). Polynomial dual energy inverse functions for bone Calcium/Phosphorus ratio determination and experimental evaluation, Appl. Radiat. Isot., 118, pp. 18-24.
[26] Koukou, V., Martini, N., Fountos, G., Michail, C., Sotiropoulou, P., Bakas, A., Kalyvas, N., Kandarakis, I., Speller, R., Nikiforidis, G. (2017). Dual energy subtraction method for breast calcification imaging, Nucl. Instrum. Meth. Phys. Res. A., 848, pp. 31-38.
[27] Koukou, V., Martini, N., Fountos, G., Michail, C., Bakas, A., Oikonomou, G., Kandarakis, I., Nikiforidis, G. (2017). Application of a Dual Energy X-ray imaging method on breast specimen, Result. Phys., 7, pp. 1734-1736.
[28] Martini, N., Koukou, V., Fountos, G., Michail, C., Bakas, A., Kandarakis, I., Speller, R., Nikiforidis, G. (2017). Characterization of breast calcification types using dual energy X-ray method, Phys. Med. Biol., 62, pp. 7741-7764.
[29] Valais, I., Kandarakis, I., Nikolopoulos, D., Michail, C., David, S., Loudos, G., Cavouras, D., Panayiotakis, G. (2007). Luminescence properties of $(Lu,Y)_2SiO_5$:Ce and Gd_2SiO_5:Ce single crystal scintillators under x-ray excitation, for use in medical imaging systems, IEEE Trans. Nucl. Sci., 54(1), pp. 11-18.
[30] Valais, I., Michail, C., David, S., Liaparinos, P., Fountos, G., Paschalis, T., Kandarakis, I., Panayiotakis, G. (2010). Comparative Investigation of Ce^{3+} doped scintillators in a wide range of photon energies covering X-ray CT, Nuclear Medicine and Megavoltage Radiation Therapy Portal Imaging applications, IEEE Trans. Nucl. Sci., 57(1), pp. 3-7.
[31] Michail, C., David, S., Liaparinos, P., Valais, I., Nikolopoulos, D., Kalivas, N., Toutountzis, A., Sianoudis, I., Cavouras, D., Dimitropoulos, N., Nomicos, C., Kourkoutas, K., Kandarakis, I., Panayiotakis, G. (2007). Evaluation of the imaging performance of LSO powder scintillator for use in x-ray mammography, Nucl. Instrum. Meth. Phys. Res. A., 580, pp. 558-561.
[32] Medical Electrical Equipment-Characteristics of Digital X-Ray Imaging Devices, Part 1: Determination of the Detective Quantum Efficiency" IEC, International Electrotechnical Commission, Geneva, Switzerland, 2003, IEC 62220-1.
[33] Medical Electrical Equipment-Characteristics of Digital X-Ray Imaging Devices - Part 1-1: Determination of the Detective Quantum Efficiency - Detectors used in radiographic imaging, IEC, International Electrotechnical Commission, Geneva, Switzerland, 2015, IEC 62220-1-1.
[34] Kandarakis, I., Cavouras, D., Panayiotakis, G., Triantis, D., Nomicos, C. (1997). An experimental method for the determination of spatial-frequency-dependent detective quantum efficiency (DQE) of scintillators used in X-ray imaging detectors, Nucl. Instrum. Meth. Phys. Res. A., 399, pp. 335-342.
[35] Kandarakis, I., Cavouras, D., Panayiotakis, G., Triantis, D., Nomicos, C. (1998). Europium-activated phosphors for use in X-ray detectors of medical imaging systems, Eur. Radiol., 8, pp. 313-318.
[36] Michail, C., Toutountzis, A., David, S., Kalivas, N., Valais, I., Kandarakis, I., Panayiotakis, G. (2009). Imaging performance and light emission efficiency of Lu_2SiO_5:Ce (LSO:Ce) powder scintillator under x-ray mammographic conditions, Appl Phys B., 95, pp. 131-139.
[37] Tombak, M., Gutan, V. (1968). Properties of a $CaWO_4$ phosphor heated in flowing hydrogen chloride, Zh. Prikl. Spektrosk., 8(5), pp. 796-802.
[38] Issler, S., Torardi, C. (1995). Solid state chemistry and luminescence of X-ray phosphors, J. Alloys Compd., 229, pp. 54-65.

[39] Michail, C. (2015). Image Quality Assessment of a CMOS/Gd_2O_2S:Pr,Ce,F X-ray Sensor, J. Sensors., 2015, pp. 874637.
[40] Buhr, E., Gunther-Kohfahl, S., Neitzel, U. (2003). Accuracy of a simple method for deriving the presampled modulation transfer function of a digital radiographic system from an edge image, Med. Phys., 30, pp. 2323-2331.
[41] Fountos, G., Michail, C., Zanglis, A., Samartzis, A., Martini, N., Koukou, V., Kalatzis, I., Kandarakis, I. (2012). A novel easy-to-use phantom for the determination of MTF in SPECT scanners, Med. Phys., 39(3), pp. 1561-1570.
[42] Karpetas, G., Michail, C., Fountos, G., Kandarakis, I., Panayiotakis, G. (2014). A new PET resolution measurement method through Monte Carlo simulations, Nucl. Med. Commun., 35(9), pp. 967-976.
[43] Karpetas, G., Michail, C., Fountos, G., Kalyvas, N., Valais, I., Kandarakis, I., Panayiotakis, G. (2017). Detective Quantum Efficiency (DQE) in PET Scanners: A Simulation Study, Appl. Radiat. Isot., 125, pp. 154-162.
[44] Samei, E., Flynn, M., Reimann, D. (1998). A method for measuring the presampled MTF of digital radiographic systems using an edge test device, Med. Phys., 25(1), pp. 102-113.
[45] Michail, C., Fountos, G., Valais, I., Kalyvas, N., Liaparinos, P., Kandarakis, I., Panayiotakis, G. (2011). Evaluation of the red emitting Gd_2O_2S:Eu powder scintillator for use in indirect X-ray digital mammography detectors., IEEE Trans. Nucl. Sci., 58(5), pp. 2503-2511.
[46] Michail, C., David, S., Bakas, A., Kalyvas, N., Fountos, G., Kandarakis, I., Valais, I. (2015). Luminescence Efficiency of $(Lu,Gd)_2SiO_5$:Ce (LGSO:Ce) crystals under X-ray radiation, Radiat. Meas., 80, pp. 1-9.
[47] Hubbell, J., Seltzer, S. (1995). Tables of X-ray mass attenuation coefficients and mass energy absorption coefficients 1 to 20MeV for elements Z=1 to 92 and 48 additional substances of dosimetric interest. US Department of commerce, NISTIR 5632.
[48] Huang, L., and Wang, M. (1995). Image thresholding by minimizing the measure of fuzziness, Pattern. Recognit., 28(1), pp. 41-51.
[49] Abramoff, M., Magalhaes, P., Ram, S. (2004). Image Processing with ImageJ, Biophoton., Int. 11(7), pp. 36-42.
[50] Hoheisel, M., Giersch, J., Bernhardt, P. (2004). Intrinsic spatial resolution of semiconductor X-ray detectors: A simulation study, Nucl. Instrum. Meth. Phys. Res. A, A531, pp. 75-81.
[51] Estribeau, M., Magnan, P. (2004). Fast MTF measurements of CMOS imagers using ISO 12233 slanted edge methodology, Proc. SPIE., 5251, pp. 243-252.
[52] Lin, C., Mathur, B., Chang, M. (2002). Analytical charge collection and MTF model for photodiode based CMOS imagers, IEEE. Trans. Electron. Devices, 49, pp. 754-761.
[53] Magnan, P. (2003). Detection of visible photons in CCD and CMOS: A comparative view, Nucl. Instrum. Meth. Phys. Res. A, 504, pp.199-212.